RSC Advances

ROYAL SOCIETY OF CHEMISTRY

www.rsc.org/advances

Journal Name

ARTICLE

Synthesis and characterization of novel luminescent europium(III) hybrid materials with a host based on titania–mesoporous silica or alumina–mesoporous silica

Received 00th January 20xx,
Accepted 00th January 20xx

DOI: 10.1039/x0xx00000x

www.rsc.org/

Xuelei Pang, Hongli Zhang, Xudong Yu, Tao Wang, Lijun Geng, Yanqiu Wang, and Yajuan Li*

Abstract: The luminescent mesoporous hybrids, Eu(M-BDA)$_2$(TTA-SBA15)$_3$ and Eu(M-BDA)$_2$(TTA-MCM41)$_3$ (M = Ti, Al), were obtained after the coordination reaction between Eu^{3+} ions and functionalized organic ligand (TTA-SBA15 or TTA-MCM41 and M-BDA (M = Ti, Al)) followed by the hydrolysis cross-linking reaction. All the mesoporous hybrids were found to retain their highly ordered mesoporous structures and possessed good thermal stability characterized by FTIR, SAXRD, TEM, N_2 adsorption–desorption curve, and TG analyses. Especially photoluminescence behaviors (e.g., photoluminescent spectra, luminescence decay analysis, and $^5D_0$ quantum efficiency) of Eu^{3+} hybrid materials were investigated in detail. Results showed that SBA-15-type mesoporous hybrids Eu(M-BDA)$_2$(TTA-SBA15)$_3$, with larger pore size than the corresponding MCM-41-type hybrids Eu(M-BDA)$_2$(TTA-SBA15)$_3$, presented longer luminescent lifetimes and higher quantum efficiency than the latter because of spatial confinements of mesoporous matrix nanochannels. The Al–O based mesoporous hybrids also exhibited more excellent luminescent properties than the corresponding Ti–O based hybrids, suggesting that the Al–O host was more beneficial to Eu^{3+} ion luminescence than the Ti–O host. The quantum efficiency of Eu(Al-BDA) (TTA-SBA15)$_3$ was even high up to 43.17%.

Introduction

As luminescent material, lanthanide (Ln) complexes have a variety of potential technological applications, such as in light-conversion molecular devices, optical amplification, fluoroimmunoassays, and organic light-emitting devices.[1] This advantage is caused by the organic ligand-sensitized complexes that combine excellent optical properties of the Ln cations such as line-shaped, long-lived, and position-defined luminescence with the characteristics of the regulated structures of complex and effective intramolecular energy transfer and strong light absorption yield from luminescent central Ln ions to the designed organic ligands (i.e., "antenna effect").[2] Therefore, Ln complexes have been extensively studied in recent decades. However, their poor thermal stabilities and low mechanical strength critically limit their practical applications. In order to solve these problems, Ln complexes are usually immobilized into stable host matrices, such as polymers, silica-based materials, natural minerals, hydroxides or liquid crystals.[3]

Among various examples reported in literature, the ordered mesoporous silica materials, such as MCM-41 and SBA-15, are promising candidate hosts for luminescent Ln complexes.[4] Inorganic mesoporous silica materials can offer rigid nanochannels and have a well-defined hydrophilic/hydrophobic phase separation that allow more sophisticated tuning of the microenvironment of Ln complexes.[5] In addition, organic ligands, which can coordinate with Ln^{3+} ions, are generally used to be covalently bond to the inorganic backbone (mainly a siloxane-based skeleton) to enhance the interactions between the mesoporous materials and the Ln complexes. Other metal oxides such as titania, zirconia, and alumina are essential functional materials, although having peculiar and fascinating physicochemical properties, few literatures regarding on these inorganic matrix hybrid systems are reported.[6] Specific organic ligand can be selected to construct the linkage between inorganic matrix and rare earth ions to solve the problem that the Ln complexes cannot be linked directly to the aluminium and titanium centres (similar to that with silicon) due to the hydrolytic cleavage of Ti–C and Al–C bonds. The different inorganic matrices have some influence on the microstructure, especially on the photophysical properties such as luminescent lifetimes and $5D_0$ quantum efficiencies. Therefore, the introduction of mixed inorganic oxides into organic–inorganic hybrid materials will probably improve these materials and thus generate new materials with more advanced properties. It is also interesting to investigate the luminescence properties of Ln complex grafted to mixed inorganic matrices compared with those of analogous silica-, titania-, or alumina-based hybrids. Besides, the concept extension to other mixed metal oxides

College of Science, and Hebei Research Center of Pharmaceutical and Chemical Engineering, Hebei University of Science and Technology, Yuhua Road 70, Shijiazhuang 050080, PR China. E-mail: liyajuan0820@163.com;
Fax: +86-311-81668548; Tel: +86-311-81668532

† Electronic Supplementary Information (ESI) available: [FTIR spectra figures, pore size distribution curves, and luminescence decay curves]. See DOI: 10.1039/ x0xx 00000x

would allow new interesting options for the development of innovative Ln^{3+}-containing inorganic–organic hybrid materials.

Combining the characteristic properties of silica backbone and the concept of specific organic ligand which can construct the linkage between titania or alumina matrix and rare earth ions, we designed and synthesized four novel Eu-titania/mesoporous silica and Eu-alumina/mesoporous silica hybrid materials. Considering that organically substituted alkoxysilanes $R'–Si(OR)_3$ can be bonded to silicon via a Si–O bond. We firstly modify the organic ligand 2-thenoyltrifluoroacetone (TTA) with silane crosslinking reagent 3-(triethoxysilyl)-propyl isocyanate (TEPIC). This process can introduce the inorganic silica matrix into hybrid materials via a covalent bond. 2, 2'-Bipyridine-4, 4'-dicarboxylic acid (BDA)[7], as multidentate N- or O-donor ligand, has been selected as the ancillary organic ligand. This compound can react with titanium alkoxide or aluminium alkoxide via the carboxylic acid group, while the heterocyclic group can coordinate with Eu^{3+} ions as well as sensitize their luminescence. Finally, the Eu luminescent inorganic–organic hybrid materials with titania/mesoporous silica or alumina/mesoporous silica based host could be obtained after the coordination reaction between Eu^{3+} ions and functionalized organic ligand. The obtained hybrid materials were structurally characterized, and their luminescence properties were examined and compared in detail.

Experimental

Materials

TEPIC, BDA, sodium hydride (NaH), tetraethoxysilane (TEOS), TTA, triblock copolymer poly(ethylene glycol)-block-poly(propylene glycol)-block-poly-(ethylene glycol) (Pluronic P123, $EO_{20}PO_{70}EO_{20}$), cetyltrimethylammonium bromide (CTAB), tetraisopropyl titanate ($Ti(OCH(CH_3)_2)_4$), and aluminium isopropoxide ($Al(OCH(CH_3)_2)_3$) were purchased from Aldrich and were used as received. Europium oxide (Eu_2O_3, 99.99%) was purchased from Shanghai Yue Long Chemical Plant. Europium nitrate was prepared as follows: Eu_2O_3 was dissolved in concentrated nitric acid, and surplus HNO_3 was removed by successive fuming. The other chemicals were all commercially available and used without further purification.

Synthesis Procedures

Synthesis of TTA-Si and TTA-functionalized SBA-15 mesoporous material (TTA-SBA15). The TTA-Si and TTA-SBA15 mesoporous material were synthesized according to the procedure described in literature.[8] Typically, 1.0 g P123 was dissolved in 7.5 g deionized water and 30 g 2 mol·L^{-1} HCl solution at 35 °C. A mixture of TEOS and TTA-Si was added into the above solution with the following molar composition: 0.0172 P123: 0.96 TEOS: 0.04 TTA-Si: 6 HCl: 208.33 H_2O. The mixture was further stirred at 35 °C for 24 h and transferred into the autoclave. The mixture was then heated at 100 °C for 48 h. The solid product was obtained by filtration, washed with deionized water, and dried at 60 °C. Removal of copolymer surfactant P123 was conducted by Soxhlet extraction with ethanol for 24 h to obtain the sample, which was denoted as TTA-SBA15.

Synthesis of TTA-functionalized MCM-41 mesoporous material (TTA-MCM41). The TTA-M41 mesoporous material were synthesized according to the procedure described in literature.[9]

Synthesis of SBA-15-type mesoporous hybrid materials Eu(M-BDA) (TTA-SBA15)$_3$ (M = Ti, Al). 10 mmol $Ti(OCH(CH_3)_2)_4$ or $Al(OCH(CH_3)_2)_3$ was added to 20 mL EtOH, which contains 5 mmol BDA, under refluxing and stirring. Afterwards, an appropriate amount of $Eu(NO_3)_3·6H_2O$ and TTA-SBA15 was added into the above solution. The final relative molar composition of the mixture was 1 $Eu(NO_3)_3·6H_2O$, 3 TTA-SBA15, 1 BDA, and 2 $Ti(OCH(CH_3)_2)_4$ or $(Al(OCH(CH_3)_2)_3)$. The stirring was continued for another 12 h to yield the precipitate. Such precipitate was recovered by filtration and extensive washing with EtOH. The resultant hybrid materials were dried at 65 °C under vacuum overnight. The detailed synthesis process and the predicted structure of Eu(BDA-Ti)$_2$ (TTA-SBA15)$_3$ is presented in Scheme 1.

Synthesis of MCM-41-type mesoporous hybrid materials Eu(M-BDA) (TTA-MCM41)$_3$ (M = Ti, Al). The synthesis procedure of Eu(M-BDA) (TTA-MCM41)$_3$ (M = Ti, Al) hybrid material was similar to that of Eu(BDA-M)$_2$(TTA-SBA15)$_3$ except that TTA-SBA15 was replaced by TTA-M41.

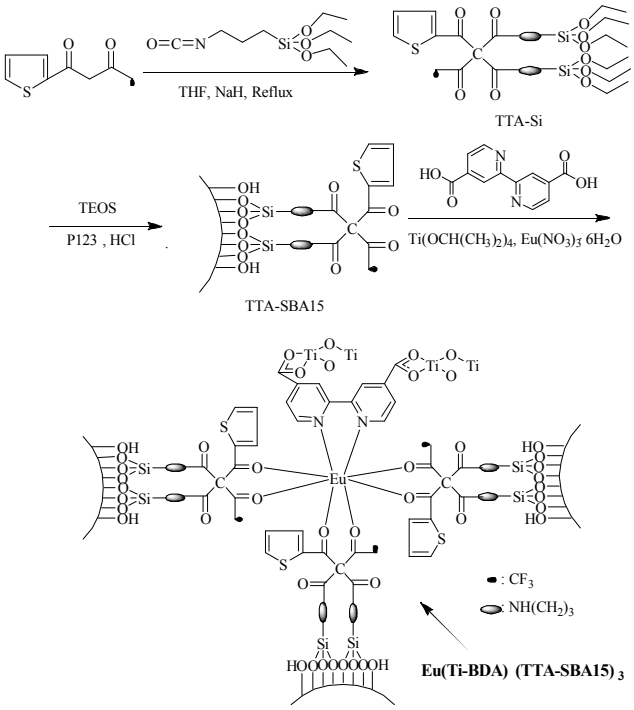

Scheme 1 Synthesis procedure of SBA-15-type mesoporous hybrid materials Eu(M-BDA) (TTA-SBA15)$_3$.

Characterization

Fourier transform infrared (FTIR) spectra were recorded within the 4000 cm^{-1} to 400 cm^{-1} region using a Nicolet model 5SXC FT-IR spectrophotometer with the KBr pellet technique. X-ray diffraction (XRD) measurements were performed using powder samples via a BRUKER D8 diffractometer (40 mA/40 kV), using monochromated Cu $K\alpha_1$ radiation (λ = 1.54 Å) in a 2θ range from 0.6° to 6°. Nitrogen

adsorption–desorption isotherms were measured at liquid nitrogen temperature using a Nova 1000 analyzer. The samples were outgassed for 3 h at 150 °C before the measurements. Surface areas were calculated by Brunauer–Emmett–Teller (BET) method. Moreover, pore size distributions were evaluated from the desorption branches of nitrogen isotherms using Barrett–Joyner–Halenda (BJH) model. The fluorescence spectra and luminescence lifetime measurements were determined on an Edinburgh fluorescence spectrometer FLS920P using a mF920H pulsed xenon flashlamp. High-resolution transmission electron microscope (HRTEM) experiments were measured on a JEOL JEM2011 transmission electron microscope that is operated at 200 kV. Thermogravimetric analysis (TGA) was performed on a Netzsch STA 409C with a heating rate of 15 °C·min^{-1} under nitrogen atmosphere.

Results and discussion

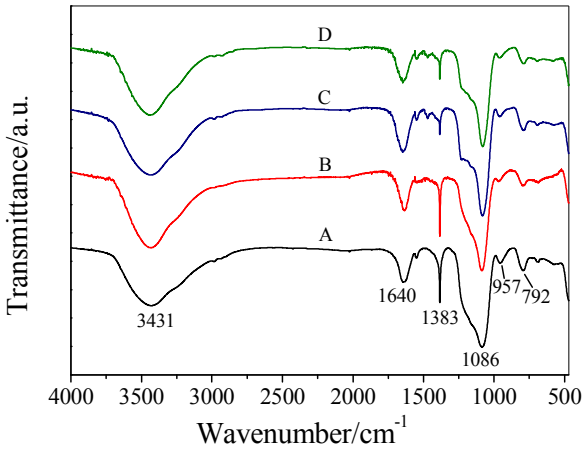

Fig. 1 FTIR spectra of as-synthesized Eu(Ti-BDA)(TTA-SBA15)$_3$ (A), Eu(Al-BDA)(TTA-SBA15)$_3$ (B), Eu(Ti-BDA)(TTA-MCM41)$_3$ (C), and Eu(Al-BDA)(TTA-MCM41)$_3$ (D).

The FTIR spectra of TTA-MCM41 and TTA-SBA15 are compared to prove successful preparation of mesoporous hybrids. The main absorptions and assignments of these hybrids are displayed in Fig. S1†. Fig. 1 shows the FTIR spectra of as-synthesized Eu-containing mesoporous hybrid materials (A for Eu(Ti-BDA)(TTA-SBA15)$_3$, B for Eu(Al-BDA)(TTA-SBA15)$_3$, C for Eu(Ti-BDA) (TTA-MCM41)$_3$, and D for Eu(Al-BDA)(TTA-MCM41)$_3$). The mesoporous hybrid materials Eu(M-BDA)(TTA-MCM41)$_3$ and Eu(M-BDA)(TTA-MCM41)$_3$ (M = Ti, Al) exhibit similar infrared absorption bands. As shown in Fig. 1, the characteristic band that appears at 1086 cm^{-1} is associated with asymmetric Si–O stretching vibration modes (ν_{as}, Si–O). Moreover, the band at 792 cm^{-1} can be attributed to the symmetric Si–O stretching vibration (ν_s, Si–O). Silanol (Si–OH) stretching vibrations of surface groups can be observed at 957 cm^{-1}. The presence of hydroxyl can be clearly evidenced by the band at 3431 cm^{-1}. In addition, The appearance of the –CONH- group at about 1640 and 1544cm^{-1} for all hybrids suggests that the functionalized organic group TTA-Si remains intact after the hydrolysis/condensation reaction and complex-grafting process. Furthermore, the band at 1383 cm^{-1} is due to the stretching vibration modes of phenyl ring of BDA, which can only be observed in Fig. 1, proving the successful introduction of BDA into hybrid materials.

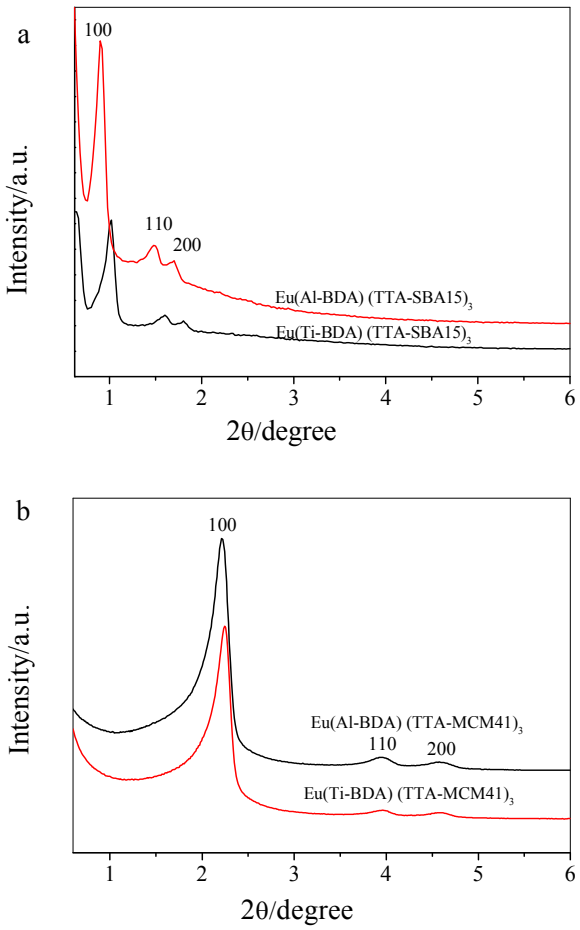

Fig. 2 SAXRD patterns of Eu(Ti-BDA) (TTA-SBA15)$_3$ and Eu(Al-BDA) (TTA-SBA15)$_3$ (a), Eu(Ti-BDA) (TTA-MCM41)$_3$ and Eu(Al-BDA) (TTA-MCM41)$_3$ (b).

The small-angle X-ray diffraction (SAXRD) patterns and nitrogen adsorption–desorption isotherms are regular and efficient methods conducted to examine highly ordered mesoporous materials. Fig. 2a shows the SAXRD patterns of mesoporous hybrid materials Eu(Ti-BDA)(TTA-SBA15)$_3$ and Eu(Al-BDA)(TTA-SBA15)$_3$. As exhibited in Fig. 2a, both of these materials display three well-resolved peaks in the 2θ range of 0.6–2°, which are marked as (100), (110), and (200) diffractions; these peaks are characteristic of SBA-15 2D hexagonal (*P6mm*) mesostructure.[10] This finding exhibits the order of the hexagonal array of two hybrid materials, which proves that the ordered hexagonal mesoporous structures of SBA-15 are almost completely conserved after the introduction of the Eu complex. For the as-synthesized Eu(Ti-BDA) (TTA-MCM41)$_3$ and Eu(Al-BDA) (TTA-MCM41)$_3$ materials (Fig. 2b), the patterns clearly show the order of the hexagonal array of the MCM-41 structure.[11] Both hybrid materials show a high-intensity (100) reflection at a low angle and two discernible order peaks (110, 200) at higher angle. The values of the corresponding unit cell parameter a_0 ($a_0 = 2d_{100}/\sqrt{3}$) of four kinds

of hybrid materials are listed in Table 1. In addition, the materials Eu(M-BDA) (TTA-SBA15)$_3$ and Eu(M-BDA) (TTA-MCM41)$_3$ all show at least three Bragg peaks, which indicates that highly ordered materials of typical MCM-41 and SBA-15 structures were obtained.

The N_2 adsorption–desorption isotherms and pore size distributions of the Eu-containing mesoporous hybrids are presented in Fig. 3 and Fig. S2 †, respectively. As presented in Fig. 3, the isotherms of these samples all show a type IV isotherm curves, which suggests typical mesoporous materials have been obtained.[12] Specific area and pore size are calculated by the Brunauer–Emmett–Teller (BET) method and Barrett–Joyner– Halenda (BJH) model, respectively. The textural parameters of the mesoporous hybrid materials are listed in Table 1. It is shown that the surface area, pore volume, and pore size of these hybrid materials, as expected, decrease after the introduction of Eu(M-BDA)TTA$_3$ (M=Ti, Al) complexes on the pore surface; thus, the organic ligand BDA has been successfully grafted into the pore channels of TTA-SBA15 and TTA-MCM41 (see ESI).[13] In addition, the SBA-15-type mesoporous hybrids Eu(M-BDA) (TTA-SBA15)$_3$ show the pore distribution at about 4.3 nm, whereas the MCM-41-type mesoporous hybrids Eu(M-BDA)(TTA-MCM 41)$_3$ display a relative narrow pore size distribution (Fig. 2S)

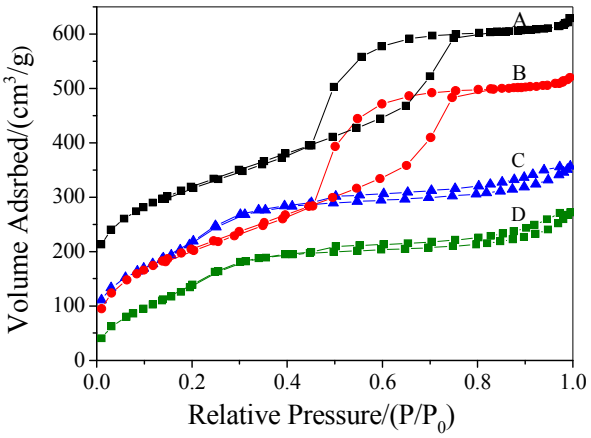

Fig. 3 N_2 adsorption–desorption isotherms of Eu(Al-BDA)(TTA-SBA15)$_3$ (A), Eu(Ti-BDA)(TTA-SBA15)$_3$ (B), Eu(Al-BDA)(TTA-MCM41)$_3$ (C), and Eu(Ti-BDA)(TTA-MCM41)$_3$ (D).

The hexagonal mesostructures of Eu(M-BDA)(TTA-SBA15)$_3$ and Eu(M-BDA)(TTA-MCM41)$_3$ are further confirmed by TEM micrographs. The general behaviors of the two materials Eu(M-BDA) (TTA-SBA15)$_3$ are similar, so are the two Eu(M-BDA)(TTA-MCM41)$_3$ hybrid materials. Therefore, only the transmission electron micrographs (TEMs) of Eu(Ti-BDA)(TTA-SBA15)$_3$ and Eu(Ti-BDA)(TTA-MCM41)$_3$ are depicted in Fig. 4. Eu(Al-BDA) (TTA-SBA15)$_3$ shows the regular hexagonal array of uniform channels, which indicate that the mesostructure of the hybrid materials can substantially be conserved after the complexation process. This finding is in agreement with the results of XRD patterns. The distance between the centers of the mesopores is estimated to be about 10 nm, which are in good agreement with the values determined from the corresponding XRD analysis (see Table 1). The level of long-range mesostructural ordering of Eu(Ti-BDA) (TTA-MCM41)$_3$ is maintained after the introduction of Eu(M-BDA) complexes on the pore surface; this finding is in agreement with the results of XRD patterns.[14] The Eu(Ti-BDA) (TTA-MCM41)$_3$ material can also be indexed on a 2D hexagonal lattice of MCM-41 materials.

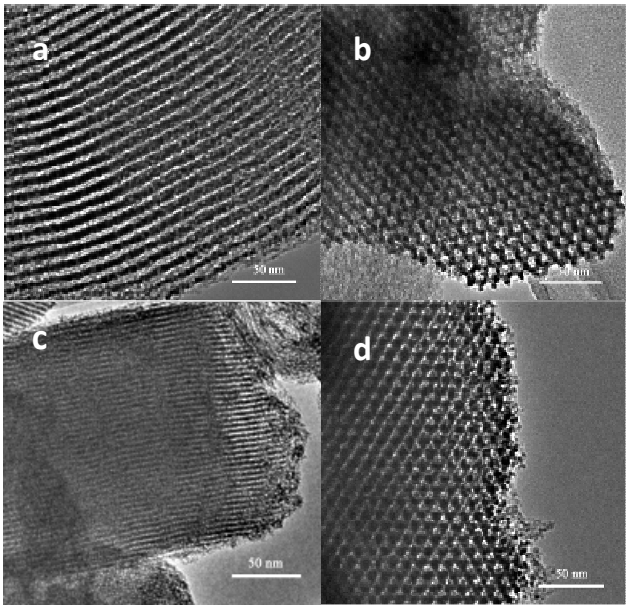

Fig. 4 TEM images of Eu(Al-BDA)(TTA-SBA15)$_3$ (a, b) and Eu(Ti-BDA)(TTA-MCM41)$_3$ (c, d); (a, c) imaged in side view and (b, d) imaged in top view, respectively.

The thermal properties of both the hybrid material Eu(Ti-BDA) (TTA-SBA15)$_3$ and pure complex Eu(M-BDA)(TTA)$_3$ have been

Table 1 Structural Parameters[a]

sample	d_{100} (nm)	a_0 (nm)	S_{BET} (m^2/g)	V (cm^3/g)	D_{BJH} (nm)	t (nm)
Eu(Al-BDA) (TTA-MCM41)$_3$	3.98	4.60	653	0.56	3.22	0.62
Eu(Ti-BDA) (TTA-MCM41)$_3$	3.93	4.54	708	0.59	3.05	0.61
Eu(Al-BDA) (TTA-SBA15)$_3$	9.72	11.22	754	0.80	4.28	1.50
Eu(Ti-BDA) (TTA-SBA15)$_3$	8.81	10.17	733	0.79	4.41	1.36

[a] d_{100} is the d(100) spacing, a_0 is the cell parameter (a_0=2 d_{100}/√3), S_{BET} is the BET surface area, V is the total pore volume, D_{BJH} is the average pore diameter, and t is the wall thickness, calculated by a_0- D_{BJH}

recorded. Fig. 5 clearly shows that Eu complex-containing hybrid material has a much higher thermal stability than the Eu(M-BDA)(TTA)$_3$ complex in the range of 30 °C to 790 °C. Below 200 °C, weight loss can be attributed to the removal of physically absorbed water and residual organic solvents. In the range of thermal decomposition temperature (350 °C to 600 °C), the weight loss of hybrid material was much lower than that of Eu complex. This fact illustrated that the inorganic host matrix will protect the organic ligand; moreover, its decomposition temperature is improved when the complex was introduced into the mesoporous material. Therefore, we can conclude that the introduction of the inorganic host matrix could increase thermal stability and may expand potential applications of the europium hybrid material.[15]

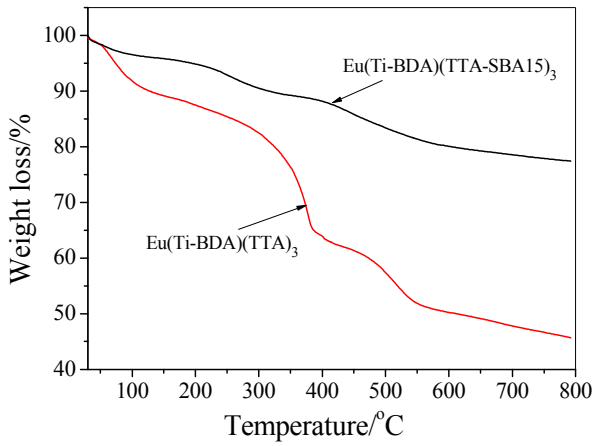

Fig. 5 Thermogravimetric analysis traces of mesoporous hybrid material Eu(Ti-BDA) (TTA-SBA15)$_3$ and pure europium complex Eu(Ti-BDA)(TTA)$_3$.

The luminescence behavior of Eu-containing mesoporous hybrid materials Eu(M-BDA)(TTA-SBA15)$_3$ and Eu(M-BDA)(TTA-MCM41)$_3$ have been investigated at room temperature. Fig. 6 presents the normalized excitation (a) and emission spectra (b) of all the mesoporous hybrid materials (A for Eu(Ti-BDA)(TTA-SBA15)$_3$, B for Eu(Al-BDA)(TTA-SBA15)$_3$, C for Eu(Ti-BDA)(TTA-MCM41)$_3$, and D for Eu(Al-BDA)(TTA-MCM41)$_3$). The excitation spectra of hybrid materials have been all obtained by monitoring the emission wavelength of Eu^{3+} ions at 614 nm and exhibit a series of broad bands between 250 and 375 nm with maximum intensity at 337, 339, 335, and 337 nm, respectively, which correspond to the efficient π-π^* transition of the ligands.[16] In addition, a narrow peak is observed at about 394 nm in the excitation spectra; this peak is ascribed to the absorption transition of *f-f* transition of Eu^{3+} ion. The *f-f* transition is weaker than the absorption of the organic ligand, which suggests the Eu^{3+} ions are essentially populated via a sensitized process, rather than by direct excitation into the intra-4f^6 lines. The typical Eu^{3+} ion emissions can be observed from the emission spectra of the hybrid materials in Fig. 6b. Bands within the 450 nm to 700 nm range can be clearly obtained, which are assigned to the $^5D_0 \rightarrow {}^7F_J$ transitions (J = J =0, 1, 2, 3 and 4, respectively) at about 579, 592, 614, 650, and 700 nm, respectively.

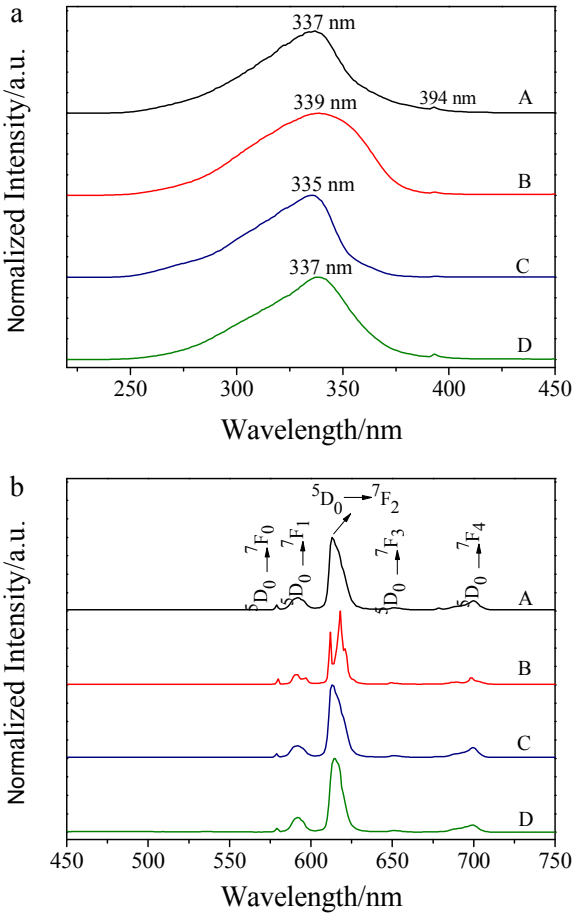

Fig 6. Room temperature excitation (a) and emission (b) spectra of the Eu-containing mesoporous hybrid materials (A for Eu(Ti-BDA)(TTA-SBA15)$_3$, B for Eu(Al-BDA)(TTA-SBA15)$_3$, C for Eu(Ti-BDA)(TTA-MCM41)$_3$, and D for Eu(Al-BDA)(TTA-MCM41)$_3$). All spectra are normalized to a constant intensity at the maximum.

The $^5D_0 \rightarrow {}^7F_2$ is allowed by the forced electric-dipole mechanism and strongly changes with the local symmetry of Eu^{3+} ions. By contrast, the $^5D_0 \rightarrow {}^7F_1$ transition, which corresponds to a parity-allowed magnetic dipole transition, is practically independent of the host material. Hence, the relative intensity ratio (R_I) of $^5D_0 \rightarrow {}^7F_2$ to $^5D_0 \rightarrow {}^7F_1$ can be considered as an indicator for the local symmetry of the europium ions.[17] Among these emission transitions of the hybrid materials, the $^5D_0 \rightarrow {}^7F_2$ transitions at about 614 nm show the strongest emission; thus, the relative intensity ratio (R_I) of $^5D_0 \rightarrow {}^7F_2$ to $^5D_0 \rightarrow {}^7F_1$ (listed in Table 2) is extremely high, indicating the chemical environment around Eu^{3+} ions is of low symmetry. By comparing the R_I values for the four mesoporous hybrids, the R_I values for Al-containing hybrid materials are higher than those of Ti-containing hybrid materials. Furthermore, the R_I values for the SBA-15-based mesoporous hybrid materials are higher than those of the MCM-41-based mesoporous hybrid materials. Therefore, different

inorganic matrices have some influence on the local symmetries of Eu^{3+} ions.

Table 2. Photoluminescent data of all mesoporous hybrid materials

	Eu(Ti-BDA) (TTA-SBA15)$_3$	Eu(Al-BDA) (TTA-SBA15)$_3$	Eu(Ti-BDA) (TTA-MCM41)$_3$	Eu(Al-BDA) (TTA-MCM41)$_3$
R_f	5.49	7.19	5.05	5.71
T (ms)	0.408	0.803	0.317	0.414
A_r	423.85	537.46	372.07	458.62
A_{nr}	2026.15	707.84	2781.93	1956.38
η(%)	17.30	43.17	11.80	18.99

The luminescence lifetimes and quantum yields are two important parameters for the efficiency estimation of the emission process of the complexes. These parameters were also determined in the current study. The decay lifetime values of $^5D_0$ excited states were measured at room temperature under the excitation wavelength that maximizes the emission intensity and were monitored by the most intense $^5D_0 \rightarrow {}^7F_2$ transitions. The luminescence decay curves of the four Eu-containing mesoporous hybrids are presented in Fig. S3†. The lifetime profiles for four samples are fitted with single exponential, indicating that all the Eu^{3+} ions locate in the same local environment in the obtained mesoporous hybrid materials. The resultant lifetime data for europium hybrids are shown in Table 2. Based on the emission spectra and lifetimes of the $^5D_0$ emitting level, the emission quantum efficiency (η) of the $^5D_0$ europium ion excited state can be determined according to the reported literature,[18] and the detailed luminescent data are presented in Table 2. Table 2 clearly shows that the SBA-15-type mesoporous hybrid materials Eu(M-BDA)(TTA-SBA15)$_3$ have longer luminescence lifetimes and higher quantum yields than the MCM-41-type mesoporous material Eu(M-BDA)(TTA-MCM41)$_3$. These outcomes may be ascribed to the following two aspects. First, the MCM-41-type mesoporous hybrids, with smaller pore volume and pore size compared with SBA-15-type mesoporous hybrids, would provide a smaller microenvironment for the Eu complexes. Therefore, the interaction between the organic ligands and the pore walls is stronger in the MCM-41-type mesoporous hybrids. This characteristic might cause a higher nonradiative transition; moreover, the photoluminescence of the europium complexes might be quenched because of the high vibration energy of hydroxyl groups on the pore wall surface.[19] Second, the relative small pore diameters of MCM-41-type mesoporous hybrids Eu(M-BDA)(TTA-MCM41)$_3$ have a significant effect on the reflection and refraction results of the Eu^{3+}-ion luminescent centre in the mesoporous channel, which affect the intramolecular energy-transfer process (from ligands to central Eu^{3+} ion). In addition, the Al–O-based mesoporous hybrids Eu(Al-BDA)(TTA-SBA15)$_3$ and Eu(Al-BDA)(TTA-MCM41)$_3$ present longer luminescent lifetimes and higher quantum efficiency than the corresponding Ti–O-based hybrids Eu(Al-BDA)(TTA-SBA15)$_3$ and Eu(Al-BDA)(TTA-MCM41)$_3$, which suggests that the Al–O host is more beneficial for the Eu^{3+} ion luminescence than the Ti–O host. We presumed that it may be due to the energy match between Al-BDA and Eu ion is much better than that between Ti-BDA and Eu ion, therefore the energy transfer efficiency between Al-BDA and Ln ion is higher that of between Ti-BDA and Eu ion.

Conclusions

In summary, four luminescent Eu-containing hybrid materials based on composite matrices of ordered mesoporous silica (SBA-15 or MCM-41) and amorphous Al (or Ti) have been designed and prepared. All resultant materials preserve their mesoscopically ordered structures and show highly uniform pore size distributions. The luminescent behaviours show that different ordered mesoporous silica and different metal oxides matrices have some influence on the microstructures, especially on the luminescence properties of the hybrid systems. First, the SBA-15-type mesoporous hybrid materials Eu(M-BDA)(TTA-SBA15)$_3$ present longer luminescence lifetimes and higher quantum yields than the corresponding MCM-41-type material Eu(M-BDA)(TTA-MCM41)$_3$, which is assigned to the spatial confinement of the mesoporous matrix. Second, the mesoporous hybrids containing Al–O network show better luminescence performance than the corresponding mesoporous materials with Ti–O network. This method allows a new interesting option for the development of rare earth hybrid materials, whose properties can be tailored by a suitable choice of the inorganic matrices and organic ligands.

Acknowledgement.

The present work is financially supported by the National Natural Science Foundation of China (No. 21401040 and No. 21301047), the Natural Science Foundation of Hebei Province (No. B2014208160, and No. B2014208091), and the Xiaoli Foundation of Hebei University of Science and Technology (2014PT75).

References

1. (a) M. D. McGehee, T. B. Bergstedt, C. Zhang, A. P. Saab, M. B. O'Regan, G. C. Bazan, V. I. Srdanov and A. J. Heeger, *Adv. Mater.,* 1999, **11**, 1349–1354.(b) J. M. Lehn, *Angew. Chem., Int. Ed. Engl.,* 1990, **29**, 1304–1319. (c) S. Okamoto, D. Vyprachticky, H. Furuya, A. Abe and Y. Okamoto, *Macromolecules,* 1996, **29**, 3511−3514. (d) C. G. Gulgas and T. M. Reineke, *Inorg. Chem.*, 2008, **47**, 1548−1559. (e) Y. J. Li, X. T. Li, X. L. Pang, X. D. Yu, X. L. Zhen, L. J. Geng and Y. Q. Wang, *Mater. Lett.*, 2015, **152** ,170-172.
2. (a) S. I. Weissman, *J. Chem. Phys.,* 1942, **10**, 214–217. (b) J.-C. G. Bünzli and C. Piguet, *Chem. Soc. Rev.,* 2005, **34**, 1048–1077. (c) D. J. Zhang, X. M. Wang, Z. A. Qiao, D. H. Tang, Y. L. Liu and Q. S. Huo, *J. Phys. Chem. C*, 2010, **114**, 12505–12510. (d) M. Q. Tan, Z. Q. Ye, G. L. Wang and J. L. Yuan, *Chem. Mater.*, 2004, **16**, 2494–2498. (e) P. Escribano, B. Julián-López, J. Planelles-Aragó, E. Cordoncillo, B. Viana, C. Sanchez, *J. Mater. Chem.*, 2008, **18**, 23–40.
3. (a) C. L. Tan and Q. M. Wang, *Inorg. Chem.*, 2011, **50**, 2953−2956. (b) C. Y. Yang, V. Srdanov, M. R. Robinson, G. C. Bazan and A. J. Heeger, *Adv. Mater.,* 2002, **14**, 980−983. (c) K. Binnemans and C. Görller-Walrand, *Chem. Rev.,* 2002, **102**, 2303−2345. (c) B. Yan, *RSC Adv.*, 2012, **2**, 9304−9324. (d) B.

Yan, Q. M. Wang, and D. J. Ma, *Inorg. Chem.,* 2009, **48**, 36−44. (e) K. Binnemans, P. Lenaerts, K. Driesen and C. Görller-Walrand, *J. Mater. Chem.,* 2004, **14**, 191−195. (f) L. D. Carlos and A. L. L. Videira, *Phys. Rev. B,* 1994, **49**, 11721−11728. (g) L.G. Li, S.Y. Feng, H. Z. Liu, *RSC Adv.*, 2014, **4**, 39132–39139. (h) Z. Zhang, G.M. Chen, J. G. Liu, *RSC Adv.*, 2014, **4**, 7991–7997.

4. (a) Y. J. Li and B. Yan, *J. Mater. Chem.*, 2011, **21**, 8129–8136. (b) Y. J. Li, B. Yan and Y. Li, *Chem. Asian J.* 2010, 5, 1642 – 1651. (c) L. N. Sun, J. B. Yu, H. J. Zhang, Q. G. Meng, E. Ma, C. Y. Peng and K. Y. Yang, *Micropor. Mesopor. Mater.,* 2007, **98**, 156−165.
5. L. N. Sun, H. J. Zhang, C. Y. Peng, J. B. Yu, Q. G. Meng, L. S. Fu, F. Y. Liu and X. M. Guo, *J. Phys. Chem. B*, 2006, **110**, 7249−7258.
6. (a) P. Liu, H. R. Li, Y. G. Wang, B. Y. Liu, W. J. Zhang, Y. J. Wang, W. D. Yan, H. J. Zhang, and U. Schubert. *J. Mater. Chem.*, 2008, **18**, 735–737. (b) H. R. Li, P. Liu, Y. G. Wang, L. Zhang, J. B. Yu, H. J. Zhang, B. Y. Liu and U. Schubert, *J. Phys. Chem. C,* 2009, **113**, 3945-3949. (c) J. Cuan and B. Yan, *RSC Adv*., 2014, **4**, 1735–1743. (e) L. Guo, B. Yan, *J. Photochem. Photobiol., A,* 2011, **224**, 141– 146. (f) C. Wang, B. Yan, J. L. Liu, L. Guo, *Eur. J. Inorg. Chem.,* 2011, 879–887.
7. (a) Y. Zuo, M. Fang, G. Xiong, P. F. Shi, B. Zhao, J. Z. Cui and P. Cheng, *Cryst. Growth Des.*, 2012, **12**,3917– 3926; (b) R. Dabestani, A. J. Bard, A. Campion, M. A. Fox, T. E. Mallouk, S. E. Webber, J. M. White, *J. Phys. Chem.*, 1988, **92**, 1872–1878.
8. Y. J. Li and B. Yan. *Inorg. Chem.*, 2009, **48**, 8276-8285.
9. B. Yan, Y. Li and B. Zhou, *Micropor. Mesopor. Mater.,* 2009, **120**, 317-324.
10. (a) D. Y. Zhao, Q. S. Huo, J. L. Feng, B. F. Chmelka and G. D. Stucky, *J. Am. Chem. Soc.*, 1998, **120**, 6024−6036. (b) D. Y. Zhao, J. L. Feng, Q. S. Huo, N. Melosh, G. H. Fredrickson, B. F. Chmelka and G. D. Stucky, *Science* 1998, **279**, 548−552.
11. C. T. Kresge, M. E. Leonowicz, W. J. Roth, J. C. Vartuli and J. S. Beck, *Nature*, 1992, **359**, 710−712.
12. J. Jarupatrakorn and T. D. Tilley, *J. Am. Chem. Soc.* 2002, **124**, 8380−8388.
13. Y. J. Li, B. Yan and Y. Li, *Micropor. Mesopor. Mater.*, 2010, **131**, 82-88.
14. J. S. Beck, J. C. Vartuli, W. J. Roth, M. E. Leonowicz, C. T. Kresge, K. D. Schmitt, C. T-W. Chu, D. H. Olson, E. W. Sheppard, S. B. McCullen,J. B. Higgins, and J. L. Schlenkert, *J . Am. Chem. Soc.*, 1992, **114**, 10837–10843.
15. K. Tang, Q. Ma, Q. Zhan and Q. Wang, *Optical Materials*, 2014, **36**, 1520–1524.
16. (a) W. H. Zhang, X. B. Lu, J. H. Xiu, Z. L. Hua, L. X. Zhang, M. Robertson, J. L. Shi, D. S. Yan and J. D. Holmes, *Adv. Funct. Mater.,* 2004, **14**, 544–552. (b) H. H. Li, S. Inoue, K. Machida and G. Adachi, *Chem. Mater.,* 1999, **11**, 3171–3176.
17. (a) P. Miranda, J. Zukerman-Schpector, P. C. Isolani, G. Vicentini and L. B. Zinner, *J. Alloys Compd.,* 2002, **344**, 141–144. (b) X. M. Guo, L. S. Fu, H. J. Zhang, L. D. Carlos, C. Y. Peng, J. F. Guo, J. B. Yu, R. P. Deng and L. N. Sun, *New J. Chem.,* 2005, **29**,1351–1358. (c) A. F. Kirby, D. Foster and F. S. Richardson, *Chem. Phys. Lett.,* 1983, **95**, 507–512.
18. (a)Y. Li, B. Yan and H. Yang, *J. Phys. Chem. C,* 2008**, 112**, 3959–3968. (b) M. H. V. Werts, R. T. F. Jukes, J. W. Verhoeven, *Phys. Chem. Chem. Phys.*, 2002, **4**, 1542–1548; (c) E. E. S. Teotonio, J. G. P. Espinola, H. F. Brito, O. L. Malta, S. F. Oliveria, D. L. A. de Faria and C. M. S. Izumi, *Polyhedron*, 2002, **21**, 1837–1844; (d) L. D. Carlos, V. D. Bermudez, R. A. S. Ferreira, L. Marques, M. Assuncao, *Chem. Mater.*, 1999, **11**, 581–588; (e) P. P. Lima, S. S. Nobre, R. O. Freire, S. A. Junior, L. Mafra, R. A. S. Ferreira, U. Pischel, O. L. Malta and L. D. Carlos, *J. Phys. Chem. C*, 2007, **111**, 17627–17634.
19. H. P. Wang, Y. F. Ma, H. Tian, N. Tang, W. S. Liu, Q. Wang and Y. Tang, *Dalton Trans.*, 2010, **39**, 7485–7492.